PHYSICAL REVIEW B VOLUME 19, NUMBER 12 15 JUNE 1979

Theory of light scattering from soft modes in IV-VI compounds

S. Katayama* and D. L. Mills
Department of Physics, University of California, Irvine, California 92717
(Received 22 September 1978)

We present a theoretical description of the Raman-Brillouin spectra from the coupled soft optical phonon and acoustical modes in IV-VI compounds. The spectra are studied above and below the cubic to rhombohedral transition temperature T_c. A mean-field description of the sublattice distortion and static strains below T_c is also given, supposing electrostrictive coupling as well as anharmonic phonon-phonon interactions are present. The theoretical results are compared with data on SnTe. We predict strong interference between the Brillouin and second-order Raman spectra above T_c. A different class of interference phenomena is present below T_c. We illustrate these points through model calculations on SnTe.

I. INTRODUCTION

The technique of light scattering has proved a powerful probe of lattice dynamics of solids for temperatures in the near vicinity of structural phase transitions.[1] In particular, there is extensive data on ferroelectric materials such as $BaTiO_3$ and KH_2PO_4, and $SrTiO_3$, where a canting of the oxygen octahedra sets in at 110 K. These experiments explore the behavior of the relevant soft optical modes and their coupling to acoustical modes as the transition temperature is approached from either above or below.

The semiconducting IV-VI compounds such as SnTe, GeTe, PbTe, and their ternary alloys are narrow-gap semiconductors which exhibit apparent ferroelectric transitions[2] as they pass from the high-temperature cubic phase to the low-temperature rhombohedral structure. Since the crystal structure in both phases is simple and the electronic band structure well studied, microscopic models of the origin of the soft optical mode associated with the phase transition have been developed, and a number of predictions compared with available data.[3]

Raman scattering experiments from the IV-VI compound semiconductors GeTe, SnTe, and $Pb_{1-x}Sn_xTe$ have been performed by several authors.[4] In particular, Sugai *et al.*[4] have succeeded in observing directly the soft optical modes in SnTe and $Pb_{1-x}Ge_xTe$ below the transition temperature. These experiments employ an Ar^+ laser with frequency well beyond the absorption edge. The soft-optical-mode frequency depends on carrier concentration, as expected from the theory set forward in Ref. 3, which invokes interband electron-phonon coupling. The near vicinity of the structural phase transition in $Sn_{1-x}Ge_xTe$ has been probed by ultrasonic methods by Rehwald and Lang,[5a] and also by Seddon and co-workers.[5b] Rehwald and Lang invoke electrostrictive coupling between the strain field of the acoustical wave and soft two-phonon states to interpret their data, which were taken above T_c.

The present paper presents the theory of light scattering from acoustical and soft optical modes in these materials, with emphasis on temperatures near T_c (both above and below) where the soft TO phonon lies low in frequency. It is then essential to take account of coupling between these excitations in this regime. One may refer to these spectra as the Raman-Brillouin spectra of the sample, since optical- and acoustical-mode contributions are simultaneously present in the same spectral regime. We shall see that the electrostrictive coupling introduced by Rehwald and Lang plays a key role in our analysis.

Before we turn to the detailed theory, we comment on the processes and mechanisms explored in the present paper. Above T_c, one has Brillouin scattering from acoustical phonons with the elasto-optical tensor providing the coupling. First-order Raman scattering from the soft TO phonon is forbidden in these rocksalt structure materials. There is coupling of the light to a *pair* of soft phonons, so there is a strongly temperature dependent second-order Raman spectrum that extends well below even $2\omega_{TO}(T)$, since the soft optical phonons are broadened by anharmonicity. The acoustical phonons couple to the lifetime-broadened two-phonon manifold via the electrostrictive terms introduced by Rehwald and Lang. This produces a contribution to the real and imaginary part of the proper self-energy of the acoustical phonon that depends strongly on both temperature and frequency. In addition, Fano interference effects occur because the photon can couple directly to the acoustic phonon, or indirectly via a process with two soft TO phonons in the intermediate state. We thus have a spectrum with rich content.

Below T_c, in the distorted phase, the light may couple directly to a single optical phonon, with a temperature-dependent matrix element. This produces a new feature in the spectrum. We also find that in the presence of scattering from the TO phonon, the integrated intensity of the total spectrum is very much greater below T_c than above T_c; the intensity drops very dramatically as one passes through T_c. The coupling to the TO phonon present below T_c thus influences not only the shape, but also the intensity of the spectrum, according to the estimates presented here.

The outline of this paper is the following. Essential ingredients for our description of light scattering in the low-temperature phase are the magnitudes and temperature variations of the order parameters. We develop a theory of these in Sec. II, and compare the results with experiments on SnTe. Section III develops the theory of light scattering both above and below T_c. We present in Sec. IV calculations for both above and below T_c, with consideration of the effect of the finite skin depth in these narrow gap materials. We also estimate the scattering intensities that can be expected.

II. TEMPERATURE VARIATION AND MAGNITUDE OF THE ORDER PARAMETERS IN THE LOW-TEMPERATURE PHASE

In the low-temperature phase of the IV-VI compounds there is a *relative* shift of the sublattices along the [111] directions. In addition, there is a rhombohedral distortion of the elementary cube as illustrated in Fig. 1. The rhombohedral angle θ is reduced below 90°. We thus have two order parameters, the angle θ, and the relative shift of the two sublattices. As we shall see, these are not independent order parameters, but are in fact linked by the electrostrictive terms present into the crystal Hamiltonian.[5]

The basic mechanism that produces the phase

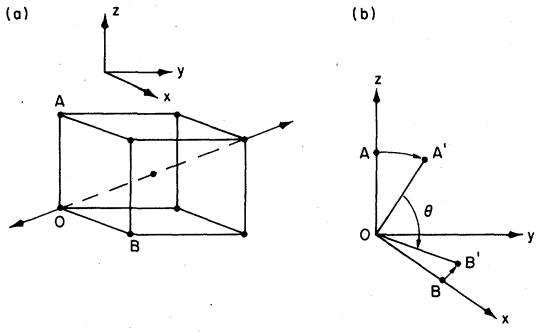

FIG. 1. Illustration of the rhombohedral distortion that is present in the low-temperature phase. This results (a) if an elementary cube is pulled by applying force along [111] so (b) the angle between OA and OB is reduced from 90° to θ.

transition is as follows. If we presume the cubic phase stable, and analyze the lattice dynamics in the harmonic approximation, then we suppose the square ω_0^2 of the TO phonon frequency is *negative*. The atomic positions thus spontaneously shift off the sites appropriate to the cubic phase to form the rhombohedral structure stable at low temperature. The magnitude of the shift in the atomic positions is controlled by the anharmonic terms included explicitly in our crystal Hamiltonian. In the distorted phase, we find the magnitude and temperature variation of the atomic displacements through use of a variational principle applied to the calculation of the free energy of the anharmonic crystal. We find the shift of the atoms off the sites appropriate to the cubic crystal decreases with increasing temperature, to vanish at a certain temperature T_c. Above T_c, the free energy is minimized with the ions on sites appropriate to the cubic phase. Thus, our theory produces a second order phase transition at T_c, with the cubic phase stable for $T > T_c$, and the rhombohedral phase below.

The calculation also yields temperature-dependent TO phonon frequencies in both the rhombohedral and the cubic phase, as we shall see. While we begin with the assumption that $\omega_0^2 < 0$, in the low-temperature phase with atoms shifted off the cubic sites, anharmonic contributions to the effective temperature-dependent force constants render the lattice stable, with all phonon frequencies positive. As T_c is approached from below, the TO phonon softens, with frequency that vanishes at T_c. In the high-temperature phase, the TO phonon frequency is again positive by virtue of anharmonic contributions to the effective force constants, to vanish as T_c is approached from above.

Before we enter the details of the theory, we comment on basic assumption that is a key feature of the analysis. This is that the displacements of the atoms off the cubic sites is a small fraction of the lattice constant. This assumption is consistent with the x-ray data cited below. This assumption enables us to begin with a Hamiltonian expressed in terms of the harmonic phonon frequencies of the (unstable) cubic lattice, and anharmonic terms with symmetry appropriate to the cubic phase. The normal coordinate of the soft TO phonon is then written as a static portion $\langle Q_{0s} \rangle$ to be found self-consistently from the variational principle, and a fluctuating part Q_{qs} that describes small oscillations about the shifted atomic positions. With this decomposition applied to the Hamiltonian appropriate to the cubic phase, below T_c when $\langle Q_{0s} \rangle \neq 0$, we are led to temperature-dependent effective force constants and tempera-

ture-dependent anharmonic coupling constants with symmetry appropriate to the low-temperature rhombohedral phase. These coupling constants are prescribed combinations of those which enter the original "bare" Hamiltonian. As one approaches T_c from below, and $\langle Q_{0s}\rangle \to 0$, the symmetry and form of the effective crystal Hamiltonian passes over to that appropriate to the cubic phase.

We turn in this section to the description of the two distortion parameters and renormalized phonon frequencies through use of a variational principle supplied to the free energy.[6] This will lead to coupled equations for the order parameters which can be solved self consistently. The Hamiltonian that forms the basis of the theory has the form

$$H = H_0 + H_s + H_{0s},$$

where H_0 describes the optical mode of the material, H_s are the acoustical strains, and H_{0s} is the coupling between them.

As a basis set, for reasons outlined above, we use the normal-mode amplitudes that characterize the high-temperature phase. The low-temperature phase is then a broken symmetry configuration describable by assigning nonzero expectation values to the relevant normal coordinates of the high-temperature configuration. The procedure is valid as long as the atomic displacements are only a small fraction of the lattice constant. We proceed by assuming that the normal coordinate for the optical mode of polarization s and wave vector $\vec{q}$ has the form

$$\tilde{Q}_{\vec{q}s} = Q_{\vec{q}s} + \delta_{\vec{q},0}\langle Q_{0s}\rangle, \tag{2.1}$$

where we later solve for $\langle Q_{0s}\rangle$ self-consistently and $Q_{\vec{q}s}$ describes fluctuations about the equilibrium configuration in the low-temperature phase. A similar relation is presumed for the strain $\epsilon_{\alpha\beta}$.

For H_0 we have

$$H_0 = \frac{1}{2}\sum_{\vec{q}s}[P^\dagger_{\vec{q}s}P_{\vec{q}s} + \omega_0^2(\vec{q}s)\tilde{Q}^\dagger_{\vec{q}s}\tilde{Q}_{\vec{q}s}] + \frac{1}{4!NV}\sum_{\{\vec{q}s\}} B_0(\{\vec{q}s\})\tilde{Q}_{\vec{q}_1s_1}\cdots\tilde{Q}_{\vec{q}_4s_4}\Delta(\vec{q}_1+\cdots+\vec{q}_4)$$

$$+\frac{1}{4NV}\sum_{\{\vec{q}js\}} B(\{q,js\})\tilde{Q}^{(a)}_{\vec{q}_1j_1}\tilde{Q}^{(a)}_{\vec{q}_2j_2}\tilde{Q}_{\vec{q}_3s_3}\tilde{Q}_{\vec{q}_4s_4}\Delta(\vec{q}_1+\cdots+\vec{q}_4). \tag{2.2}$$

Where $\omega_0(\vec{q}s)$ is the bare harmonic phonon frequency, and the second term describes four-phonon coupling between the long-wavelength optical modes that will concern us. The harmonic phonon frequency $\omega_0^2(\vec{q}s)$ is negative at $\vec{q}=0$, when s refers to one of the TO modes. In the long-wavelength limit, the cubic symmetry of the high-temperature phase causes the three-phonon term to vanish when all three modes have $\vec{q}$ near zero. Here the symbol $B_0(\{\vec{q}s\})$ is an abbreviation for $B_0(\vec{q}_1s_1,\ldots,\vec{q}_4s_4)$ and $B(\{\vec{q},js\})$ is an abbreviation for $B(\vec{q}_1j_1,\vec{q}_2j_2,\vec{q}_3s_3,\vec{q}_4s_4)$. The coupling constants B_0 thus control the interaction between four long-wavelength optical modes (B_0), and two long-wavelength optical modes with two acoustical modes of polarization j_1 and $j_2(B)$.

The long-wavelength acoustical waves that "freeze in" to produce the rhombohedral distortion are split off for explicit consideration. These modes are described by the combination of

$$H_s = \frac{1}{2}V\sum_{\substack{\alpha\beta\\ \gamma\delta}} c_{\alpha\beta\gamma\delta}\tilde{\epsilon}_{\alpha\beta}(\vec{q})^*\tilde{\epsilon}_{\gamma\delta}(\vec{q}) + E_{\rm kin}, \tag{2.3}$$

with

$$\tilde{\epsilon}_{\alpha\beta}(\vec{q}) = \delta_{\vec{q},0}\langle\epsilon_{\alpha\beta}\rangle + \epsilon_{\alpha\beta}(\vec{q})$$

and

$$H_{s0} = \frac{1}{2}\sum_{\substack{\alpha\beta\\ \gamma\delta}}\sum_{\vec{q}_1\cdots\vec{q}_3} \Phi_{\alpha\beta\gamma\delta}(\vec{q}_1;\vec{q}_2s_2,\vec{q}_3s_3)\epsilon_{\alpha\beta}(\vec{q}_1) \times \hat{e}_\gamma(\vec{q}_2s_2)\hat{e}_\delta(\vec{q}_3s_3) \times \tilde{Q}_{\vec{q}_2s_2}\tilde{Q}_{\vec{q}_3s_3}\Delta(\vec{q}_1+\vec{q}_2+\vec{q}_3) \tag{2.4}$$

where $E_{\rm kin}$ is the kinetic energy of the acoustical motions of the lattice.

Equation (2.4) is written in such a form that the coupling constant $\Phi_{\alpha\beta\gamma\delta}$ remains finite in the limit as all three wave vectors $\vec{q}_1, \vec{q}_2$, and $\vec{q}_3$ vanish. The term H_{s0} is the electrostrictive coupling that plays a key role in the paper by Rehwald and Lang.[5a]

We treat the thermodynamics of the system through use of the variational principle applied to the Helmholtz free energy F. This may be done by computing F using the trial density matrix

$$\rho_{\rm eff} = \exp(-\beta H_{\rm eff})/{\rm Tr}[\exp(-\beta H_{\rm eff})], \tag{2.5}$$

$$H_{\rm eff} = E_0 + \frac{1}{2}\sum_{\vec{q}s}[P^\dagger_{\vec{q}s}P_{\vec{q}s} + \bar{\omega}^2(\vec{q}s)Q^\dagger_{\vec{q}s}Q_{\vec{q}s}], \tag{2.6}$$

where E_0 is a constant, $\bar{\omega}(\vec{q}s)$ and $\langle Q_{0s}\rangle$ are the temperature-dependent variational parameters to be found by requiring

$$F = {\rm Tr}(\rho_{\rm eff}H) + (1/\beta){\rm Tr}(\rho_{\rm eff}\ln\rho_{\rm eff}) \tag{2.7}$$

to be an extremum with respect to variations in these parameters. The strain variables $\epsilon_{\alpha\beta}(\vec{q})$ are here replaced by their static values $\delta_{\vec{q},0}\langle\epsilon_{\alpha\beta}\rangle$, with $\langle\epsilon_{\alpha\beta}\rangle$ also variational parameters. The fluctuations $\epsilon_{\alpha\beta}(\vec{q})$ about $\langle\epsilon_{\alpha\beta}\rangle$ produce the light scattering that will be the topic of the remaining sections of the paper.

Use of the above trial density matrix yields the mean-field estimate for the free energy given by $F_m - TS$, where

$$
\begin{aligned}
F_m = {} & \frac{1}{2}\sum_{s}\omega_0^2(0s)\langle Q_{0s}\rangle^2 + \frac{1}{2}\sum_{\vec{q}s}\omega_0^2(\vec{q}s)\langle Q^{\dagger}_{\vec{q}s}Q_{\vec{q}s}\rangle + \frac{1}{2}\sum_{qs}\hbar\omega(qs)(n_{\vec{q}s}+\tfrac{1}{2}) \\
& + \frac{1}{4NV}\sum_{\vec{q}s}\left(\sum_{j}B(\vec{q}j,0s)\langle Q^{(a)\dagger}_{\vec{q}j}Q^{(a)}_{\vec{q}j}\rangle + \sum_{s_1}B_0(\vec{q}s_1,0s)\langle Q^{\dagger}_{\vec{q}s_1}Q_{\vec{q}s_1}\rangle\right)\langle Q_{0s}\rangle^2 \\
& + \frac{1}{24NV}\sum_{s}B_0(0s,0s)\langle Q_{0s}\rangle^4 + \frac{1}{4NV}\sum_{\vec{q}j}\sum_{\vec{q}'s}B(\vec{q}j,\vec{q}s)\langle Q^{(a)\dagger}_{\vec{q}j}Q^{(a)}_{\vec{q}j}\rangle\langle Q^{\dagger}_{\vec{q}'s}Q_{\vec{q}'s}\rangle \\
& + \frac{1}{8NV}\sum_{\vec{q}s}\sum_{\vec{q}'s'}B_0(\vec{q}s,\vec{q}'s')\langle Q^{\dagger}_{\vec{q}s}Q_{\vec{q}s}\rangle\langle Q^{\dagger}_{\vec{q}'s'}Q_{\vec{q}'s'}\rangle + \frac{1}{2}V\sum_{\substack{\alpha\beta\\\gamma\delta}}c_{\alpha\beta\gamma\delta}\langle\epsilon_{\alpha\beta}\rangle\langle\epsilon_{\gamma\delta}\rangle \\
& + \frac{1}{2}\sum_{\substack{\alpha\beta\\\gamma\delta}}\sum_{s}\Phi_{\alpha\beta\gamma\delta}(0;0s,0s)\hat{e}_{\gamma}(0s)\hat{e}_{\delta}(0s)\langle Q_{0s}\rangle^2\langle\epsilon_{\alpha\beta}\rangle \\
& + \frac{1}{2}\sum_{\substack{\alpha\beta\\\gamma\delta}}\sum_{\vec{q}s}\Phi_{\alpha\beta\gamma\delta}(0;-\vec{q}s,\vec{q}s)\hat{e}_{\gamma}(\vec{q}s)\hat{e}_{\delta}(\vec{q}s)\langle Q^{\dagger}_{\vec{q}s}Q_{\vec{q}s}\rangle\langle\epsilon_{\alpha\beta}\rangle,
\end{aligned}
\tag{2.8a}
$$

and finally the entropy S,

$$
S = k_B\sum_{\vec{q}s}\left[(1+n_{\vec{q}s})\ln(1+n_{\vec{q}s}) - n_{\vec{q}s}\ln n_{\vec{q}s}\right]. \tag{2.8b}
$$

In Eq. (2.8a), we use an abbreviated notation with $B_0(\vec{q}s,\vec{q}'s')$ in place of $B_0(-\vec{q}s,\vec{q}s,-\vec{q}s',\vec{q}s')$ and permutations. A similar abbreviated notation is used for the other coupling constants, in the interest of simplicity. In these expressions,

$$
n_{\vec{q}s} = \{\exp[\hbar\tilde{\omega}(qs)/k_BT] - 1\}^{-1}
$$

and

$$
\langle Q^{\dagger}_{\vec{q}s}Q_{\vec{q}s}\rangle = [\hbar/\tilde{\omega}(\vec{q}s)](n_{\vec{q}s}+\tfrac{1}{2}). \tag{2.9}
$$

We now restrict our attention to the selected class of displacements $\langle Q_{0s}\rangle$ and distortions $\langle\epsilon_{\alpha\beta}\rangle$ known to be important in the IV-VI compounds. We demonstrate that this set gives a minimum in F. The [111] relative displacement of the sublattices is described by freezing in a TO mode in the following manner. Let $\hat{e}(\vec{q}s)$ be the eigenvector, normalized to unity, for the optical mode of wave vector $\vec{q}$ and polarization s. Let $\vec{q}\to 0$ along a direction perpendicular to the [111] direction, and assign to the TO mode polarized along [111] the static displacement

$$
e_x(0x)\langle Q_{0s}\rangle = e_y(0s)\langle Q_{0s}\rangle = e_z(0s)\langle Q_{0s}\rangle \equiv \langle Q_0\rangle/\sqrt{3}.
$$

The rhombohedral strain is described by presuming $\langle\epsilon_{xy}\rangle = \langle\epsilon_{yz}\rangle = \langle\epsilon_{zx}\rangle \equiv \langle\epsilon\rangle$, with other $\langle\epsilon_{\alpha\beta}\rangle$ equal to zero.

A variation of the free energy with respect to $\langle Q_0\rangle$, $\langle\epsilon\rangle$, and $\tilde{\omega}(qs)$, respectively leads to the three conditions, with $\omega_0^2(0s) = \omega_0^2$. The first is

$$
\begin{aligned}
\langle Q_0\rangle\Bigg(\omega_0^2 & + \frac{1}{2NV}\sum_{\vec{q},s_1}B_0(qs_1,0s)\langle Q^{\dagger}_{\vec{q}s_1}Q_{\vec{q}s_1}\rangle \\
& + \frac{1}{2NV}\sum_{\vec{q}j}B(\vec{q}j,0s)\langle Q^{(a)\dagger}_{\vec{q}j}Q^{(a)}_{\vec{q}j}\rangle \\
& + \frac{1}{6NV}B_0(0s,0s)\langle Q_0\rangle^2 + 2\Phi_c(0)\langle\epsilon\rangle\Bigg) = 0,
\end{aligned}
\tag{2.10a}
$$

where

$$
\Phi_c(0) = \frac{1}{2}\sum_{\alpha\beta\gamma\delta}\Phi_{\alpha\beta\gamma\delta}(0;0s,0s)\hat{e}_{\gamma}(0s)\hat{e}_{\delta}(0s),
$$

and the sum on α, β, γ, and δ includes only those combinations for which $\langle\epsilon_{\alpha\beta}\rangle$ is nonvanishing. Then we have

$$
\begin{aligned}
& 12Vc_{44}\langle\epsilon\rangle + \Phi_c(0)\langle Q_0\rangle^2 \\
& \quad + \sum_{\vec{q}s_1}\Phi_c(\vec{q}s_1)\langle Q^{\dagger}_{\vec{q}s_1}Q_{\vec{q}s_1}\rangle = 0,
\end{aligned}
\tag{2.10b}
$$

with

$$
\begin{aligned}
\Phi_c(\vec{q}s_1) = {} & \frac{1}{2}\sum_{\alpha\beta\gamma\delta}\Phi_{\alpha\beta\gamma\delta}(0,-\vec{q}s_1,\vec{q}s_1) \\
& \times \hat{e}_{\gamma}(-\vec{q}s_1)\hat{e}_{\delta}(\vec{q}s_1).
\end{aligned}
$$

Finally, we get for $\tilde{\omega}(\vec{q}s)$ the result

$$
\begin{aligned}
\tilde{\omega}^2(\vec{q},s) = {} & \omega_0^2(qs) + \frac{1}{2NV}B_0(0s,\vec{q}s)\langle Q_0\rangle^2 \\
& + \frac{1}{2NV}\sum_{\vec{q}'j}B(\vec{q}'j,\vec{q}s)\langle Q^{(a)\dagger}_{\vec{q}'j}Q^{(a)}_{\vec{q}'j}\rangle \\
& + \frac{1}{2NV}\sum_{\vec{q}'s'}B_0(\vec{q}'s,\vec{q}'s)\langle Q^{\dagger}_{\vec{q}'s'}Q_{\vec{q}'s'}\rangle \\
& + 2\Phi_c(\vec{q}s)\langle\epsilon\rangle.
\end{aligned}
\tag{2.10c}
$$

We have to solve this set of equations in a self-consistent manner. Before we do so, a brief comment on the nature of the results is in order.

The quantity $\omega(\vec{q}s)$ is the renormalized phonon frequency, with temperature variation produced by anharmonicity, and force-constant changes produced by the shifts in atomic positions when $\langle\epsilon\rangle$ and $\langle Q_0\rangle$ are nonvanishing.

Note that below T_c, when $\langle Q_0\rangle \neq 0$, Eqs. (2.10a) and (2.10c) may be combined to give

$$\lim_{\vec{q}\to 0} \omega(\vec{q}s)^2 = \frac{B_0(0s,0s)}{3NV}\langle Q_0\rangle^2 . \tag{2.11}$$

With $B_0(0s,0s) > 0$, an assumption necessary to produce the phase transition, Eq. (2.11) shows that in the low-temperature phase, the TO phonon frequency is positive definite, to vanish as T_c is approached from below. Anharmonicity has stabilized the lattice.

If Eq. (2.10b) is used to eliminate $\langle\epsilon\rangle$ from Eq. (2.10a), and if we define new effective coupling constants

$$\tilde{B}_0 = B_0(0s,0s) - N\Phi_c^2(0)/2c_{44} \tag{2.12a}$$

and

$$\tilde{B}_0(\vec{q}s_1) = B_0(\vec{q}s_1, 0s_1) - N\frac{\Phi_c(0)\Phi_c(\vec{q}s_1)}{6c_{44}} , \tag{2.12b}$$

we then solve for $\langle Q_0\rangle$:

$$\langle Q_0\rangle^2 = \frac{6NV}{\tilde{B}_0}\left(-\frac{1}{2NV}\sum_{\vec{q}j} B(\vec{q}j,0s)\langle Q^{(a)\dagger}_{\vec{q}j} Q^{(a)}_{\vec{q}j}\rangle - \omega_0^2 + \frac{1}{2NV}\sum_{\vec{q}s_1} \tilde{B}_0(\vec{q}s_1)\langle Q^{\dagger}_{\vec{q}s_1} Q_{\vec{q}s_1}\rangle\right) . \tag{2.13}$$

Equation (2.13) is a self-consistent equation from which one may determine $\langle Q_0\rangle$. The order parameter $\langle Q_0\rangle$ enters the right-hand side in the average $\langle Q^{\dagger}_{\vec{q}s} Q_{\vec{q}s}\rangle$, as one sees by noting the long-wavelength behavior of $\omega(\vec{q}s)$ given in Eq. (2.11). However, our estimates show that the influence of the third term on the right-hand side of Eq. (2.13) is very small, except possibly extremely close to T_c. Even though $\langle Q^{\dagger}_{qs} Q_{qs}\rangle$ becomes large as $\vec{q}\to 0$ near T_c where $\langle Q_0\rangle$ is small, $\langle Q^{\dagger}_{\vec{q}s} Q_{\vec{q}s}\rangle$ is large only over a very small volume of phase space. Note that the third term on the right-hand side remains finite even if we set $\langle Q_0\rangle \equiv 0$. We ignore this term, and Eq. (2.13) then gives $\langle Q_0\rangle$ directly, and we need not solve for it self-consistency.

The phase transition occurs as follows. As discussed earlier, ω_0^2 is negative, and at temperature $T=0$, the quantity in large parentheses in Eq. (2.13) is positive. With $\tilde{B}_0$ assumed positive, we have a finite distortion $\langle Q_0\rangle$ at $T=0$. As T increases, $\langle Q^{(a)\dagger}_{\vec{q}j} Q^{(a)}_{\vec{q}j}\rangle$ increases, to drive $\langle Q_0\rangle^2$ to zero at a transition temperature defined by the vanishing of the quantity in large parentheses. For $\tilde{B}_0 > 0$, the transition is second order. The sum over $\vec{q}$ may be evaluated by choosing a Debye spectrum for the acoustical modes. We replace $B(\vec{q}\,{}^{0}_{s})$ by an average coupling constant B to find

$$\langle Q_0\rangle^2 = \frac{9\hbar^2}{k_B\Theta_D^2}\frac{B}{\tilde{B}_0}[\varphi(T_c) - \varphi(T)] \equiv 12\overline{M}NVa_0^2\delta^2 \tag{2.14a}$$

with

$$\varphi(T) = \frac{T^2}{2\Theta_D}\int_0^{\Theta_D/T} dx\, x\coth(\tfrac{1}{2}x) . \tag{2.14b}$$

The second statement of Eq. (2.14a) defines a dimensionless parameter δ,[7] introduced by earlier authors,[8] that provides a measure of the relative shift of the two sublattices in the rhombohedral phase. In Eq. (2.14a), a_0 is the lattice constant and $\overline{M}$ is the reduced mass of the unit cell. Note that $\varphi(T)$ is defined so that $\varphi(T) \equiv T$ when $T \gg \Theta_D$. From Eq. (2.14a), it is evident that $\langle Q_0\rangle^2$ vanishes as T_c is approached from below.

The strain parameter $\langle\epsilon\rangle$ is related to $\langle Q_0\rangle$ by Eq. (2.10b). We may again ignore the terms in $\langle Q^{\dagger}_{\vec{q}s} Q_{\vec{q}s}\rangle$ for reasons outlined earlier, and necessarily $\Phi_c(0)$ is negative for a solution to the coupled equations to occur. Thus,

$$\langle\epsilon\rangle = [\,|\Phi_c(0)|/12Vc_{44}]\langle Q_0\rangle^2 . \tag{2.15}$$

From Eqs. (2.14), it is evident that $\langle Q_0\rangle$ vanishes like $(T_c - T)^{1/2}$, in the manner characteristic of mean-field theory. However, $\langle\epsilon\rangle$ vanishes not as $(T_c - T)^{1/2}$, but rather as the first power $(T_c - T)$.

We next compare the predictions of the model with experimental data. Iizumi *et al.* have reported neutron scattering determinations of the dimensionless displacement parameter δ.[8] In Fig. 2(a), we reproduce his data (circles) and compare with the prediction of Eq. (2.14a). We have chosen $\Theta_D = 120$ K, the transition temperature $T_c = 100$ K, $\overline{M}N = 1.631$ g/cm^3, $a_0 = 6.321$ Å, and finally from the fit we determine that

$$B/\tilde{B}_0 = 0.43 . \tag{2.16}$$

To choose the value of $B/\tilde{B}_0$, we fit the data close to T_c. We also plotted the temperature variation of δ for $T_c = 75$ K in the broken line using the same parameters with one for solid line.

Given $\langle Q_0\rangle$, from Eq. (2.15), we can calculate $\langle\epsilon\rangle$, and in fact determine $|\Phi_c(0)|$ from the measured magnitude of the rhombohedral angle θ in Fig. 1. One has $\theta = 90° - 2\langle\epsilon\rangle$. From an analysis of x-ray diffraction data, Muldawer[9] has inferred values of $\langle\epsilon\rangle$ for powder samples. If we choose $|\Phi_c(0)| = 2.1\times 10^{27}$ sec^{-2}, then we obtain the broken curve in Fig. 2(b) from the broken line in Fig. 2(a).

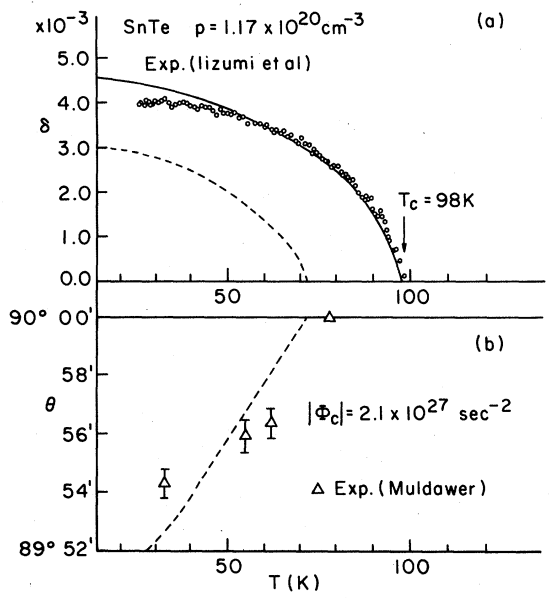

FIG. 2. (a) Data of Iizumi *et al.* on the sublattice distortion parameter δ for SnTe, as a function of temperature. (b) Rhombohedral angle θ as a function of temperature, from the data of Muldawer.

This calculation is in good accord with the points reported by Muldawer, although the lowest temperature point lies somewhat off our curve. Unfortunately, Muldawer's reported T_c is lower than the generally accepted value of $\approx$100 K by a substantial amount, indicating free carries may be present in his sample.[3] Clearly, however, our value of $|\Phi_c(0)|$ gives $\langle\epsilon\rangle$ close to the required magnitude.

The parameters determined from the fit to data on δ and $\langle\epsilon\rangle$ will be employed in the light scattering calculations reported below.

III. THEORY OF LIGHT SCATTERING FROM SOFT MODES IN IV-VI COMPOUNDS

This section describes the theory of light scattering from the soft TO phonon and acoustical phonons in the near vicinity of the structural phase transition described in Sec. II. We consider temperatures above and below the ordering temperature T_c; a key feature of our theory is the role of coupling between these sets of modes provided by crystal anharmonicity, in the form of the electrostrictive coupling introduced in Sec. II in our description of the lattice statics. Here, in essence we explore the influence of this coupling on the dynamical properties of the lattice.

We set up the theory of light scattering in two steps. First, we suppose the material transparent to the incident radiation, a condition unlikely to be met in experiments on these compounds. With the scattering efficiency found in this manner, a simple convolution procedure using theory developed for light scattering from opaque materials by one of the present authors and his collaborators,[10] and later by Inoue and Moriya,[11] leads one to results that incorporate the role of the finite skin depth. We shall see that the strong absorption of the visible radiation, with the consequent uncertainty in wave vector components normal to the surface, dramatically modifies the line shapes appropriate to a transparent material. At visible frequencies used in typical light scattering studies, the (small gap) IV-VI compounds are strongly absorbing, with skin depths of at most a few hundred angstrom.

The differential scattering efficiency is defined as the fraction of photons scattered per unit solid angle per unit frequency interval. This scattering efficiency S has the form

$$\frac{d^2S}{d\Omega_s d\omega_s} = \left(\frac{\omega_s}{c}\right)^4 \frac{\omega_0}{\omega_s} \int_{-\infty}^{+\infty} \frac{d\tau}{2\pi} e^{-i(\omega_0-\omega_s)\tau} \times \langle \alpha^*_{\mu\nu}(\vec{Q},t)\alpha_{\mu\nu}(\vec{Q},t+\tau)\rangle , \tag{3.1}$$

where $d\Omega_s$ is the element of solid angle, ω_0 and ω_s are the frequency of the incident and scattered light, and $\alpha_{\mu\nu}(\vec{Q},t)$ is the fluctuating part of the electric susceptibility of the material. This describes modulation of the susceptibility by fluctuations of wave vector $\vec{Q}=\vec{k}_0-\vec{k}_s$, where $\vec{k}_0$ and $\vec{k}_s$ are the wave vectors of the incident and scattered light. More precisely, if $\alpha_{\mu\nu}(\vec{r},t)$ is the amplitude of the fluctuating susceptibility at position $\vec{r}$, then

$$\alpha_{\mu\nu}(\vec{Q},t) = \int d^3r\, e^{-i\vec{Q}\cdot\vec{r}}\alpha_{\mu\nu}(\vec{r},t) . \tag{3.2}$$

To begin, we need the form of $\alpha_{\mu\nu}(\vec{r},t)$. As in our description of the lattice dynamics that formed the basis for Sec. II, we presume all atomic displacements (including the static displacements below T_c) are small, and expand about the equilibrium positions in the high temperature cubic phase. Then if we write, in a continuum theory, the optical displacement as $\bar{u}_\sigma(\vec{r}) = \langle u_\sigma\rangle + u_\sigma(\vec{r})$ and the dynamic part of the strain as $\epsilon_{\mu\nu}(\vec{r})$,

$$\alpha_{\mu\nu}(\vec{r}t) = \frac{1}{2}\sum_{\sigma\rho} A_{\mu\nu\sigma\rho}u_\sigma(\vec{r})u_\rho(\vec{r}) + \sum_{\sigma\rho} A_{\mu\nu\sigma\rho}\langle u_\sigma\rangle u_\rho(\vec{r}) + \sum_{\gamma\delta} K_{\mu\nu,\gamma\delta}\epsilon_{\gamma\delta}(\vec{r}) , \tag{3.3}$$

where $A_{\mu\nu\sigma\rho}$ and $K_{\mu\nu,\gamma\delta}$ may be related to second and first derivatives of the electronic polarizability with atomic displacement.

We note right away that in the high-temperature cubic phase where $\langle u_\sigma \rangle$ vanishes, first-order Raman scattering by the soft TO phonon is forbidden [second term in Eq. (3.3)]. We do have scattering by two-phonon processes that extends to very low frequencies near T_c (first term). By virtue of the electrostrictive terms that couple the acoustical strain into the two-phonon manifold, we shall find interference effects above T_c in the Brillouin–second-order Raman spectrum. Below T_c, first-order scattering is also allowed, and the other processes remain.

We expand $u_\sigma(\vec{r})$ in terms of normal coordinates $Q_{\vec{q}s}$, with interest only in values of $\vec{q}$ near the zone center:

$$u_\sigma(\vec{r}) = \frac{1}{(N\bar{M}V)^{1/2}} \sum_{\vec{q}s} \hat{e}_\sigma(\vec{q}s) Q_{\vec{q}s} e^{i\vec{q}\cdot\vec{r}} \tag{3.4}$$

For the dynamical strains,

$$\epsilon_{\sigma\rho}(\vec{r}) = \frac{1}{2} \sum_{\vec{q}j} i\,[q_\sigma \hat{e}_\rho(\vec{q}j) + q_\rho \hat{e}_\sigma(\vec{q}j)] \times \frac{Q^{(a)}_{\vec{q}j}}{(\rho V)^{1/2}} e^{i\vec{q}\cdot r} . \tag{3.5}$$

Throughout this section, s serves as an optical mode index and j an acoustical-mode index.

We can then cast the expression for $\alpha_{\mu\nu}(\vec{Q}, t)$ in the form

$$\begin{aligned}\alpha_{\mu\nu}(\vec{Q}, t) = &\sum_{\vec{q}'} \sum_{ss'} a_{\mu\nu}(\vec{Q} - \vec{q}'s, \vec{q}'s') \\ &\times Q_{\vec{Q}-\vec{q}'s}(t) Q_{\vec{q}'s'}(t) \\ &+ 2 \sum_{s,s'} a_{\mu\nu}(0s, \vec{Q}s') \langle Q_{0s} \rangle Q_{\vec{Q}s'}(t) \\ &+ \sum_j b_{\mu\nu}(\vec{Q}j) Q^{(a)}_{\vec{Q}j}(t) .\end{aligned} \tag{3.6}$$

We do not write out the coefficients $a_{\mu\nu}(\vec{q}s, \vec{q}'s')$ and $b_{\mu\nu}(\vec{Q}j)$ explicitly, since they are obtained straightforwardly from the quantities displayed above.

When the form given for $\alpha_{\mu\nu}(\vec{Q}, t)$ is inserted into the scattering efficiency, nine terms result. Again, we do not write these out in full. In Fig. 3, we provide an illustration of the basic processes incorporated into the theory. In a previous paper,[12] it was noted that from examination of the imaginary part of the photon proper self-energy, one may obtain the Raman cross section. In Fig. 3, we show the basic contributions to the photon proper self-energy included in our present treatment.

The diagram (i) in Fig. 3 describes Raman scattering by two soft TO phonons, diagram (ii) Brillouin scattering by an acoustical mode, and diagram (iii) shows interference between the one-phonon and two-phonon manifold (Fano interference) produced by the presence of electrostrictive coupling. Of course, there is also a diagram not shown that has the two TO phonons created at the left vertex. Below T_c, the additional processes shown in Fig. 3(b) contribute. First-order Raman scattering is now allowed [diagram (v)], there is coupling between the acoustical mode and the soft TO phonon [diagram (vi)], and interference between a single TO phonon, and the two-TO-phonon manifold which overlap the TO-phonon spectral density in frequency, when damping is present.

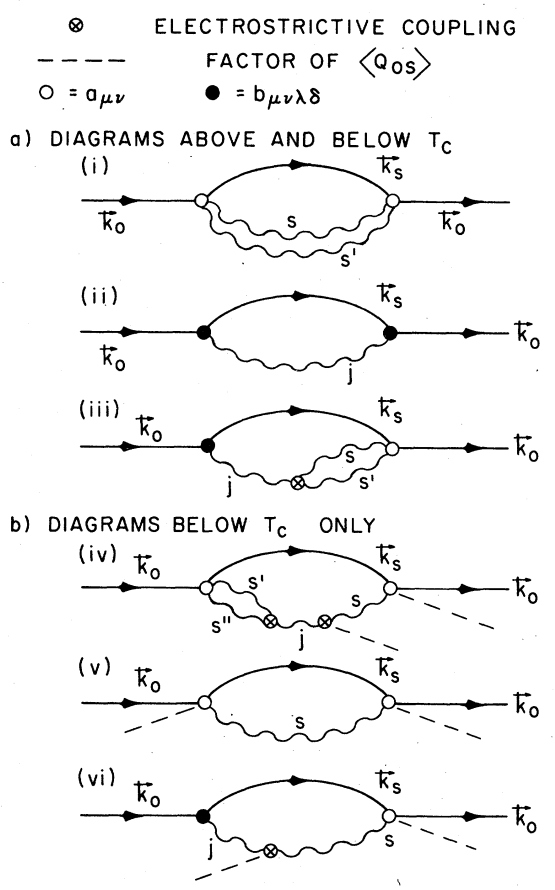

FIG. 3. Illustration of the contribution to the photon self-energy from the basic scattering processes incorporated into the present theory. (a) Diagrams that contribute both above and below T_c and (b) diagrams that contribute only below T_c.

To calculate the scattering efficiency, we require the following Green's functions:

$$D_{jj'}(\vec{Q}, \tau) = \langle T(Q^{(a)\dagger}_{\vec{Q}j}(\tau) Q^{(a)}_{\vec{Q}j'}(0)) \rangle , \tag{3.7a}$$

$$D_{ss'}(\vec{Q}, \tau) = \langle T(Q^{\dagger}_{\vec{Q}s}(\tau) Q_{\vec{Q}s'}(0)) \rangle , \tag{3.7b}$$

$$D_{ss';j}(\vec{q}, \vec{Q} - \vec{q}; \vec{Q}; \tau) = \langle T(Q^{\dagger}_{\vec{q}s}(\tau) Q^{\dagger}_{\vec{Q}-\vec{q}s'}(\tau) Q^{(a)}_{\vec{Q}j}(0)) \rangle , \tag{3.7c}$$

$$D_{ss's''}(\vec{q},\vec{Q}-\vec{q},\vec{Q};\tau) = \langle T(Q^{\dagger}_{\vec{q}s}(\tau)Q^{\dagger}_{\vec{Q}-\vec{q}s'}(\tau)Q^{*}_{\vec{Q}s}(0))\rangle , \quad (3.7d)$$

$$D_{sj}(\vec{Q},\tau) = \langle T(Q^{\dagger}_{\vec{Q}s}(\tau)Q^{(a)}_{\vec{Q}j}(0))\rangle , \quad (3.7e)$$

$$D_{ss',tt'}(\vec{q},\vec{Q}-\vec{q},\vec{q}'',Q-\vec{q}'';\tau) = \langle T(Q^{\dagger}_{\vec{q}s}(\tau)Q^{\dagger}_{\vec{Q}-\vec{q}'s'}(\tau)Q_{\vec{Q}-\vec{q}''t'}(0)Q_{\vec{q}''t}(0))\rangle . \quad (3.7f)$$

The correlation functions in Eqs. (3.7) may be calculated within the framework of the imaginary-time many-body formalism. Then the relevant spectral densities may be formed and related to the light scattering cross section. We have proceeded through use of the diagrammatic approach, focusing attention on the role of the electrostrictive coupling between the acoustical modes, and the long-wavelength optical phonons. It is straightforward to solve the set of coupled Dyson equations produced by this analysis. Rather than write out the full details, we sketch how the calculation proceeds through illustrating first the diagrams included. Then we discuss the various propagators that enter.

The diagrams included in the present analysis are illustrated in Figs. 4 and 5. The encircled crosses denote the electrostrictive coupling and the dashed line the factor of $\langle Q_{0s}\rangle$ that controls the mixing between the acoustical and optical branches below T_c. In propagator s, we use the Green's function that describes a soft TO phonon with dispersion relation

$$\tilde{\omega}^2_{\mathrm{TO}}(q,T) = \omega^2_{\mathrm{TO}}(T) + Aq^2 . \quad (3.8)$$

In Sec. II, we developed a microscopic theory of the temperature-dependent soft TO phonon. Here we regard A as an adjustable temperature-independent parameter.

We also include damping in the soft-TO-phonon propagator by taking its spectral density to be Lorentzian, centered at $\tilde{\omega}_{\mathrm{TO}}(q,T)$, with phenomenological halfwidth $\Gamma(T)$; in the interest of simplicity we take $\Gamma(T)$ independent of frequency and wave vector. In the numerical work reported below, we adjusted $\Gamma(T)$ to reproduce the width of the TO mode far enough below T_c that mixing with acoustical modes is unimportant. We comment on this in more detail below.

In Fig. 4(a), we show the diagrams that contribute to the acoustical-phonon Green's function introduced in Eq. (3.7a). Note that in the renormalized optical phonon propagator described in Fig. 4(b), the internal acoustical-phonon line is described by a propagator that differs from the full propagator in Fig. 4(a). If this distinction is not drawn, then certain diagrams which involve $\langle Q_{0s}\rangle$ are double counted.

To describe the Green's functions produced by the above analysis, one introduces the coupling constants

$$g_j(ss') = \frac{1}{2}\sum_{\substack{\alpha\beta\\ \eta\nu}} \Phi_{\alpha\beta\eta\nu}(\vec{q}_1;0s,0s') \times \hat{e}_{\alpha\beta}(\hat{q}_1)\hat{e}_{\eta}(0s)\hat{e}_{\nu}(0s') , \quad (3.9)$$

where $\Phi_{\alpha\beta\eta\nu}(\vec{q}_1;0s,0s')$ is the limit of $\Phi_{\alpha\beta\eta\nu}(\vec{q}_1;\vec{q}_2 s,\vec{q}_3 s')$ [Eq. (2.4)] as all three wave vectors vanish. In principle, the resulting object depends on the directions of $\vec{q}_1$, $\vec{q}_2$, and $\vec{q}_3$ in this limit. We shall always encounter the square of the coupling constant $g_j(s,s')$ here, and in the square we construct an angular averaged coupling constant by replacing the squares of the optical eigenvectors by the average of these squares over a solid angle, treating the average on $\vec{q}_2$ and $\vec{q}_3$ as independent. These averaged coupling constants still depend on

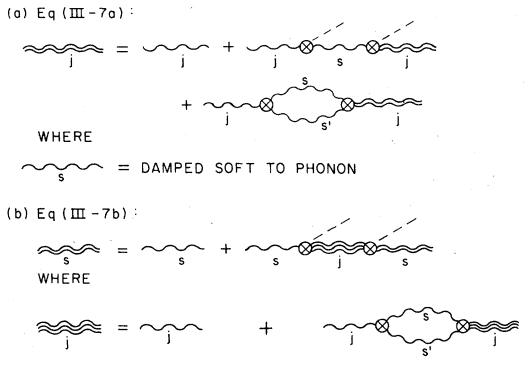

FIG. 4. Diagrams which contribute to the acoustical-phonon Green's function defined in Eq. (3.7a). The encircled cross denotes the electrostrictive coupling, as in Fig. 3. (b) Diagrams that contribute to the optical phonon propagator defined in Eq. (3.7b).

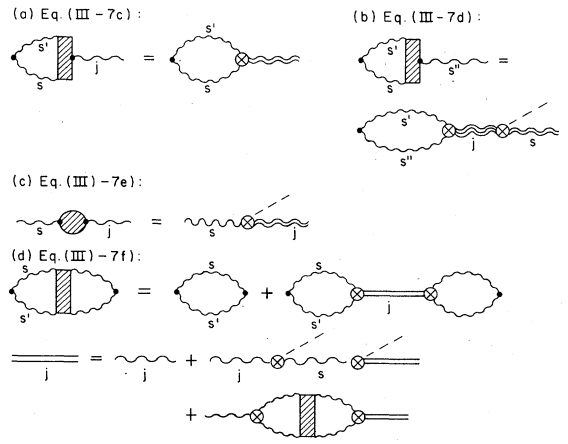

FIG. 5. Diagrams which contribute to the propagators defined in (a) Eq. (3.7c), (b) Eq. (3.7d), (c) Eq. (3.7e), and (d) Eq. (3.7f).

the polarization of the acoustical phonon j through the explicit retention of the factor $\hat{e}_{\alpha\beta}(\hat{q}_1)$, which depends on both the direction of $\vec{q}_1$ and the polarization of the mode as $\vec{q}_1 \to 0$.

In the imaginary-time representation, the Fourier transform $D_{jj}(\vec{Q}, i\omega_n)$ of the propagator in Eq. (3.7a) is, from Fig. 4(a)

$$D_{jj}(\vec{Q}, i\omega_n) = [D_j^{(0)}(\vec{Q}, i\omega_n)^{-1} - \Pi_j(\vec{Q}, i\omega_n)]^{-1} \tag{3.10a}$$

where $\omega_n = (2\pi n/\hbar\beta)$, the self-energy $\Pi_j(Q, i\omega_n)$ is

$$\begin{aligned}\Pi_j(\vec{Q}, i\omega_n) = {} & 4\sum_{ss'} |g_j(s,s')|^2 \langle Q_{0s}\rangle^2 \\ & \times D_{s'}^{(0)}(\vec{Q}, i\omega_n) \\ & + \frac{2}{\beta}\sum_{\substack{\vec{q}ss' \\ i\omega_m}} |g_j(s,s')|^2 D_s^{(0)}(\vec{q}, i\omega_m) \\ & \times D_{s'}^{(0)}(\vec{Q}-\vec{q}, i\omega_n - i\omega_m), \end{aligned} \tag{3.10b}$$

and also

$$D_j^{(0)}(\vec{Q}, i\omega_n) = [\omega_j^2(\vec{q}) + \omega_n^2]^{-1}, \tag{3.10c}$$

with $D_s^{(0)}(\vec{Q}, i\omega_m)$ constructed as outlined above.

For the propagator in Eq. (3.7b), we have

$$D_{ss'}(\vec{Q}, i\omega_n) = \delta_{ss'}[D_s^{(0)}(\vec{Q}, i\omega_n)^{-1} - \Pi_s(\vec{Q}, i\omega_n)]^{-1}, \tag{3.11a}$$

where

$$\begin{aligned}\Pi_s(\vec{Q}, i\omega_n) = {} & 4\sum_j \sum_{s'} |g_j(ss')|^2 \langle Q_{0s'}\rangle^2 \\ & \times D_j(\vec{Q}, i\omega_m), \end{aligned} \tag{3.11b}$$

where

$$\begin{aligned} D_j(\vec{Q}, i\omega_m) = \Big(& D_j^{(0)}(\vec{Q}, i\omega_n)^{-1} \\ & - \frac{2}{\beta}\sum_{\vec{q}} \sum_{s's''} |g_j(s's'')|^2 D_{s'}^{(0)}(\vec{q}, i\omega_m) \\ & \times D_{s''}^{(0)}(\vec{Q}-\vec{q}, i\omega_n - i\omega_m)\Big)^{-1}. \end{aligned} \tag{3.11c}$$

In terms of the quantities introduced above, the Fourier transforms of the remaining Green's functions become

$$D_{ss';j}(\vec{q}, \vec{Q}-\vec{q}; \vec{Q}; i\omega_n) = -g_j(s,s')\frac{2}{\beta}\sum_{i\omega_m} D_s^{(0)}(\vec{q}, i\omega_m) D_{s'}^{(0)}(\vec{Q}-\vec{q}, i\omega_n - i\omega_m) D_{jj}(\vec{Q}, i\omega_n), \tag{3.12}$$

$$\begin{aligned} D_{ss's''}(\vec{q}, \vec{Q}-\vec{q}, \vec{Q}; i\omega_n) = {} & \sum_j g_j(s,s')\frac{2}{\beta}\sum_{i\omega_m, \vec{q}} D_s^{(0)}(\vec{q}, i\omega_m) \\ & \times D_{s'}^{(0)}(\vec{Q}-\vec{q}, i\omega_n - i\omega_m) 2\sum_{s'''} D_j(\vec{Q}, i\omega_n)\langle Q_{0s'''}\rangle g_j(s''', s'') D_{s'''s''}(\vec{Q}, i\omega_n), \end{aligned} \tag{3.13}$$

$$D_{sj}(\vec{Q}, i\omega_n) = -D_s^{(0)}(\vec{Q}, i\omega_n)^2 \sum_{s'} g_j(ss')\langle Q_{0s'}\rangle D_{jj}(\vec{Q}, i\omega_n), \tag{3.14}$$

and finally,

$$\begin{aligned} D_{ss',tt'}(\vec{q}, \vec{Q}-\vec{q}, \vec{q}'', \vec{Q}-\vec{q}''; i\omega_n) = {} & D_{ss',tt'}^{(0)}(\cdots, i\omega_n) \\ & + \sum_j g_j(ss') g_j^*(tt') D_{jj}(\vec{Q}, i\omega_n) \frac{4}{\beta^2}\Big(\sum_{i\omega_m} D_s^{(0)}(\vec{q}, i\omega_m) D_{s'}^{(0)}(\vec{Q}-\vec{q}, i\omega_n - i\omega_m)\Big) \\ & \times \Big(\sum_{i\omega_{m'}} D_t^{(0)}(\vec{q}'', i\omega_{m'}) D_{t'}^{(0)}(\vec{Q}-\vec{q}'', i\omega_n - i\omega_{m'})\Big), \end{aligned} \tag{3.15}$$

with the lowest-order contribution to the two-phonon propagator $D_{ss',tt'}^{(0)}(\cdots, i\omega_n)$

$$\begin{aligned} D_{ss',tt'}^{(0)}(\cdots, i\omega_n) = {} & \frac{1}{\beta}\sum_{i\omega_m} D_s^{(0)}(\vec{q}, i\omega_m) D_{s'}^{(0)}(\vec{Q}-\vec{q}, i\omega_n - i\omega_m) \\ & \times (\delta_{st}\delta_{s't'}\delta_{\vec{q}\vec{q}'} + \delta_{st'}\delta_{s't}\delta_{\vec{q}', \vec{Q}-\vec{q}}). \end{aligned} \tag{3.16}$$

This completes the calculation of the various propagators that enter our description of the light scattering. The final step is to combine all these into a formula for the scattering efficiency. Again, we do not reproduce the algebra, in the interest of brevity. When the scattering efficiency is written out, it is proportional to the quantity

$$\mathcal{S}(\vec{Q}, \Omega) = \sum_{\gamma\gamma'} \sum_{\beta\beta'} \hat{e}_{\gamma'}^*(s)\hat{e}_\gamma(s)\hat{e}_{\beta'}^*(I)\hat{e}_\beta(I)\mathcal{S}_{\gamma'\gamma,\beta'\beta}(\vec{Q}, \Omega), \tag{3.17}$$

where $\hat{e}(s)$ and $\hat{e}(I)$ are the polarization vectors of the scattered and incident light. It is $\delta(\vec{Q}, \Omega)$ that controls the behavior of the light scattering cross section, and we leave off prefactors insensitive to the frequency shift Ω of the light, and its wave vector transfer $\vec{Q}$. We have

$$\begin{aligned} \mathcal{S}_{\gamma'\gamma,\beta'\beta}(\vec{Q}, \Omega) = {} & 2\hbar[1+n(\Omega)]\sum_j \sum_s \mathrm{Im}[\Gamma_{\gamma'\beta',js}^*(\Omega - i\epsilon) \\ & \times \Gamma_{\beta\gamma,js}(\Omega + i\epsilon) \\ & \times D_{jj}(\vec{Q}, \Omega + i\epsilon)], \end{aligned} \tag{3.18}$$

where $D_{jj}(\vec{Q},\Omega+i\epsilon)$ is the analytic continuation of $D_{jj}(\vec{Q},i\omega_n)$ [Eq. (3.10a)] from the imaginary axis to just above the real axis in the Ω plane. In Eq. (3.18), $n(\Omega)$ is the Bose-Einstein function $n(\Omega)=[\exp(\hbar\Omega/k_BT)-1]^{-1}$, and

$$\Gamma_{\beta\gamma,js}(\Omega+i\epsilon)=b_{\beta\gamma j}-4\sum_{s'}\alpha_{\beta\gamma}(0s',\vec{Q}s)\,g_j(ss')\langle Q_{0s'}\rangle^2 D_s^{(0)}(\vec{Q},\Omega+i\epsilon)$$
$$-\frac{2}{\beta}\sum_{\vec{q}',i\omega_m}\alpha_{\beta\gamma}(\vec{Q}-\vec{q}'s',\vec{q}s)D_s^{(0)}(\vec{q}',i\omega_m)D_s^{(0)}(\vec{Q}-\vec{q}',\Omega+i\epsilon-i\omega_m)g_j(s's)\,. \tag{3.19}$$

With these formulas, one may examine the light scattering spectrum, as a function of frequency shift Ω and wave vector transfer $\vec{Q}$. These results assume the material is transparent. As remarked earlier, the light scattering experiments will be carried out under conditions where the sample is opaque to the incident radiation. In a simple backscattering measurement, with incident light at normal incidence, the spectrum for scattering from the opaque substrate is readily calculated. One takes $\vec{Q}$ directed normal to the surface, with $\hat{e}(s)$ and $\hat{e}(I)$ parallel to it. Note that $\hat{e}(s)$ and $\hat{e}(I)$ may be either parallel or perpendicular to each other. We discuss the backscattering selection rules explicitly in Sec. IV, for specific geometries. Given the relevant components of $\mathcal{S}_{\gamma'\gamma,\beta'\beta}(\hat{n}Q,\Omega)$, with $\hat{n}$ normal to the surface, one performs the convolution operation

$$\mathcal{S}_{\gamma'\gamma,\beta'\beta}(\Omega)=\int_0^{+\infty}\frac{dQ}{2\pi}\frac{1}{|Q+\kappa_z^{(i)}+\kappa_z^{(s)}|^2}$$
$$\times\,\mathcal{S}_{\gamma'\gamma,\beta'\beta}(Q\hat{n},\Omega) \tag{3.20}$$

where $\kappa_z^{(i)}$ and $\kappa_z^{(s)}$ are the complex wave vectors of the incident and scattered radiation in the substrate.

In Sec. IV, we present a series of numerical studies of the light scattering spectrum for SnTe, for the cases where the substrate is transparent and where it is opaque.

IV. NUMERICAL STUDIES OF BRILLOUIN-RAMAN SPECTRA FOR SnTe NEAR T_c

We present here our results of numerical studies of the light scattering spectrum from SnTe near T_c, using the theory developed in Secs. I–III. We predict the form of the Brillouin-Raman spectrum with emphasis on the influence of interference between the acoustical phonons and the low-lying two-phonon continuum associated with the soft TO modes near T_c. Below T_c, we have also the first order scattering from the soft TO mode which, as we have seen, is added into the interference structure below T_c.

The calculation is performed in the following two steps:

(i) We suppose the following: (a) We probe only the cubic (001), (111) surfaces above T_c and rhombohedral (001) surface below T_c of SnTe with $T_c=100$ K. We consider only a monodomain crystal with c axis along the [111] direction below T_c. (b) The sample is transparent for Ar^+ laser line (5145 Å). (c) The laser light is incident normally on the surface and is scattered with scattering angle 180° (backward scattering), and the polarization of scattered photon is parallel or perpendicular to that of incident light.

(ii) We take into accout the effect of the opacity of the medium which is met in actual experiments with visible radiation. By simple convolution procedure mentioned in Sec. III, the second-stage calculation smears out the interference structure of the lines and spreads the spectrum over the entire frequency range, with strong temperature dependence. In Table I, we show the selection rules for relevant modes obtained by examining the symmetry properties for elasto-optical tensor p_{ij} as well as Raman tensor components.

A. Line-shape function under transparent conditions

1. Behavior above T_c

We examine the scattering spectrum from (001) surface. According to Table I, the longitudinal-acoustical (LA) mode with wave vector parallel to the z axis is only allowed for the $z(xx)\bar{z}$ configuration. The expression for the lineshape function due to this mode is derived from Eq. (3.18). After tedious rearrangement of the formula, the spectrum can be written

$$\mathcal{S}_{\rm LA}(Q,\Omega)=2\hbar[1+n(\Omega)]\,\frac{Q^2}{4\rho}$$
$$\times K_{12}^2[1+L(\omega_{\rm LA}^2-\Omega^2)]^2(\hat{\epsilon}_{zz})^2$$
$$\times\left(-\,\mathrm{Im}\,\frac{1}{\Omega^2-\omega_{\rm LA}^2+(Q^2/4\rho)g_{\rm LA}^2\Pi_0(Q,\Omega)}\right), \tag{4.1}$$

where

$$L=-\tfrac{1}{9}[(A_{11}+A_{12})\Phi_{12}+A_{12}\Phi_{11}]\rho V/K_{12}Q^2g_{\rm LA}^2\,, \tag{4.2a}$$

$$g_{\rm LA}^2=\tfrac{1}{9}(2\Phi_{12}^2+\Phi_{11}^2)\,, \tag{4.2b}$$

TABLE I. Selection rules and summary of parameters in cubic SnTe and rhombohedral SnTe.

$\vec{K}_1$	$\vec{K}_s$	$\vec{Q}$	$\hat{\xi}$	Mode	ρv^2	$I_0^{\perp\perp}$	$I_0^{\perp\parallel}$
			[001]	LA	c_{11}	p_{12}^2	0
				TA1	c_{44}	0	0
Cubic	[001]	[001]					
				TA2	c_{44}	0	0
				TO	⋮	0	0
			[111]	LA	$\frac{1}{3}(c_{11}+2c_{12}+4c_{44})$	$\frac{1}{9}(p_{11}+2p_{12}-2p_{44})^2$	0
				TA1	$\frac{1}{3}(c_{11}-c_{12}+c_{44})$	$\frac{1}{18}(p_{11}-p_{12}-2p_{44})^2$	0
	[111]	[111]		TA2	$\frac{1}{3}(c_{11}-c_{12}+c_{44})$	0	$\frac{1}{18}(p_{11}-p_{12}-2p_{44})^2$
				TO	⋮	0	0
			[001]	LA	c_{33}^r	p_{12}^2	0
				TA1	c_{44}^r	p_{14}^2	0
Rhombohedral	[001]	[001]					
				TA2	c_{44}^r	0	p_{14}^2
			$E(-x)$ [a]	TO1		0	$-c$
			$E(y)$ [a]	TO2		c	0

[a] From R. Loudon, Adv. Phys. 13, 423 (1964).

and the quantity K_{ij} is related to the elasto-optical tensor as $K_{ij} = -\epsilon_\infty^2 p_{ij}$, with ϵ_∞ the optical dielectric constant.

In deriving Eq. (4.1), we neglect the terms with origin in the imaginary part of K_{ij} as well as the terms corresponding to the pure second order process which separates out of the spectrum as a distinct contribution. Thus, we include only the scattering from the acoustical mode, with its proper self-energy affected strongly by electrostrictive coupling to the two-phonon manifold. The quantities A_{ij} and Φ_{ij} represent the components of the second-order Raman tensor and of electrostrictive coupling tensor, respectively, with abbreviation of index in the ordinary manner (i.e., the notation is the same as that used in elasticity theory.)

From Eq. (A8) in the Appendix, the proper self energy function $\Pi_0(Q,\Omega)$ is, for our model,

$$\mathrm{Re}\Pi_0(Q,\Omega) = \frac{k_B T}{4\pi}\left(1+\Gamma^2\frac{\Omega^2-4\Gamma^2}{(\Omega^2+4\Gamma^2)^2}\right) \times \frac{1}{\omega_0(T)A^{3/2}}\,, \tag{4.3a}$$

$$\mathrm{Im}\Pi_0(Q,\Omega) = -\frac{k_B T}{4\pi}\frac{4\Omega\Gamma^3}{(\Omega^2+4\Gamma^2)^2} \times \frac{1}{\omega_0(T)A^{3/2}}\,, \tag{4.3b}$$

where $\Gamma(T)$ represent the halfwidth of the soft TO phonon. We have taken the limit $Q \to 0$ on the right-hand side.

In the scattering geometry $z(xy)\bar{z}$, we have the contribution from the second-order scattering, not contained in Eq. (4.1),

$$\mathcal{S}_{2\mathrm{TO}} = 2\hbar[n(\Omega)+1]\tfrac{1}{9}(A_{44})^2[-\mathrm{Im}\Pi_0(Q,\Omega)]\,. \tag{4.4}$$

We turn now to the discussion of the scattering spectra from the (111) surface. In order to abbreviate the complex combination of the fourth rank tensors, we set up new coordinates $(x'y'z')$, where x', y', and z' axes are parallel to the $[1\bar{1}0]$, $[11\bar{2}]$, and $[111]$ crystal axes, respectively. The line-shape function for the LA and the transverse-acoustical (TA) modes allowed in the $z'(x'x')\bar{z}'$ scattering geometry is given by

$$\mathcal{S}_j(Q,\Omega) = 2\hbar[1+n(\Omega)]\frac{Q^2}{4\rho} \times K_j^2[1+L_j'(\omega_j^2-\Omega^2)]^2(\epsilon_j)^2 \times\left(-\mathrm{Im}\frac{1}{\Omega^2-\omega_j^2+(Q^2/4\rho)g_j'^2\Pi_0(Q,\Omega)}\right). \tag{4.5}$$

When the index j refers to the LA mode, we have

$$K_{\mathrm{LA}} = \tfrac{1}{3}(K_{11} + 2K_{12} - 2K_{44}) , \tag{4.6a}$$

$$\epsilon_{\mathrm{LA}} = \hat{\epsilon}_{z'z'} , \tag{4.6b}$$

$$L'_{\mathrm{LA}} = -\frac{[(A_{1'1'} + A_{1'2'})\Phi_{3'1'} + \Phi_{3'3'} A_{1'3'}]\rho V}{9K_{\mathrm{LA}} Q^2 g'^2_{\mathrm{LA}}} , \tag{4.6c}$$

and

$$g'^2_{\mathrm{LA}} = \tfrac{1}{9}(\Phi^2_{3'3'} + 2\Phi^2_{3'1'}) . \tag{4.6d}$$

For TA mode, we have

$$K_{\mathrm{TA}} = (1/\sqrt{18})(K_{11} - K_{12} - 2K_{44}) , \tag{4.7a}$$

$$\epsilon_{\mathrm{TA}} = 2\hat{\epsilon}_{y'z'} , \tag{4.7b}$$

$$L'_{\mathrm{TA}} = -\frac{[(A_{1'1'} - A_{1'2'})\Phi_{4'1'} + 2A_{1'4'}\Phi_{4'4'}]\rho V}{9K_{\mathrm{TA}} Q^2 g'^2_{\mathrm{TA}}} , \tag{4.7c}$$

and

$$g'^2_{\mathrm{TA}} = \tfrac{2}{9}(\Phi^2_{4'1'} + \Phi^2_{4'4'}) . \tag{4.7d}$$

The corresponding one from the TA mode for the $z'(x'y')\bar{z}'$ scattering geometry may be obtained from (4.7a)–(4.7d) by replacing the polarization vector component $2\hat{\epsilon}_{y'z'}$ by $2\hat{\epsilon}_{x'z'}$. Since the formulas contain quite a number of parameters (second-order Raman tensor, elasto-optical tensor, electrostrictive coupling constant, soft-phonon halfwidth), we have to choose the appropriate value for each parameter in the most reasonable way. Hopefully, future experiments will enable us to refine these initial estimates. Rehwald and Lang[5a] experimentally evaluated the ratio of the electrostrictive coupling constants γ_a, γ_e, and γ_t on $Sn_{1-x}Ge_xTe$ with value of x between 0.09 and 0.25. The quantities γ_a, γ_e, and γ_t are the coupling constants between a pair of soft modes and the dilational, tetragonal, and rhombohedral strain, respectively. Their evaluated values give the ratios $\gamma_a:\gamma_e:\gamma_t = 0.437:0.348:1$. By employing these values we can estimate the ratio of the electrostrictive coupling constants in our notation as

$$\Phi_{11}:\Phi_{12}:\Phi_{44} = 1.797:0.405:1 ,$$

where Φ_{44} is equivalent to $\frac{1}{2}\Phi_c$ introduced in Sec. II. The value of $|\Phi_c|$ is 2.1×10^{27} sec^{-2} which we estimate by reproducing the magnitude of the observed rhombohedral angle, as displayed in Fig. 2 and discussed earlier in the present paper. The elasto-optical tensor components are chosen in the following way. A recent theoretical calculation[13] provides us the value of the rate of change of the refractive index (n) with density (ρ) for SnTe. Then from this we can estimate the numerical value $\frac{1}{3}(p_{11}+2p_{12})$ through the relation

$$\frac{p_{11}+2p_{12}}{3} = \frac{2}{\epsilon_\infty^{3/2}}\,\rho\frac{dn}{d\rho} .$$

Assuming the same value for the ratio $p_{11}:p_{12}:p_{44} = 1.22:1:\frac{1}{9}$ as KI (Ref. 14) with NaCl-type structure, we have $p_{11} = -0.0407$, $p_{12} = -0.496$, and $p_{44} = -0.00623$. This choice for the relative values of the elasto-optical tensor is the least certain in our choice of numerical parameters, in our view. We comment below on the role this choice plays in our calculated spectra.

The remaining parameters such as the second-order Raman tensor and soft-phonon halfwidth are chosen so the halfwidth of the calculated spectrum agrees with the observed one at 45 K on SnTe.[4] The values of parameters estimated as above as well as other parameters require in the computations are listed in Table II.

In Figs. 6 and 7, we plot the function $I_j(Q,\Omega)$ defined by

$$I_j(Q,\Omega) = (4\rho/2\hbar Q^2\epsilon_j^2)S_j(Q,\Omega) , \tag{4.8}$$

for the wave number $Q = 0.865\times10^6$ cm^{-1}.

In Fig. 6(a) the curves show the temperature dependence of the scattering spectrum due to the LA mode from the (001) surface. There is a strong temperature dependence in its peak position and

TABLE II. Values of physical parameters of SnTe.

Density	ρ	6.51 (g cm^{-3})	Soft-mode dispersion coefficients	A	1.63×10^{10} (cm^2 sec^{-2})[a]
refractive index	n	3.54 for 5145 Å[b]		α	8.883×10^{22} (sec^{-2} K^{-1})[c]
	K	4.20 for 5145 Å[b]			
Elastic tensor components	c_{11}	10.93×10^{11} (dyn cm^{-2})[d]	Electrostrictive coupling constants	g_{LA}	0.933×10^{27} (sec^{-2})
	c_{12}	0.21×10^{11} (dyn cm^{-2})[d]		g'_{LA}	1.092×10^{27} (sec^{-2})
	c_{44}	0.97×10^{11} (dyn cm^{-2})[d]		g'_{TA}	0.567×10^{27} (sec^{-2})
Γ (at 50 K)		2 (cm^{-1})			
Γ (at 90 K)		3.4 (cm^{-1})		$\Phi_{4'4'}$	1.184×10^{27} (sec^{-2})

[a] S. Katayama, Solid State Commun. 19, 381 (1976).
[b] M. Cardona and D. L. Greenaway, Phys. Rev. 133, A1635 (1964).
[c] S. Sugai, K. Murase, and H. Kawamura, Solid State Commun. 23, 127 (1977).
[d] T. Seddon, S. C. Gupta, and G. A. Saunders, Solid State Commun. 20, 69 (1976).

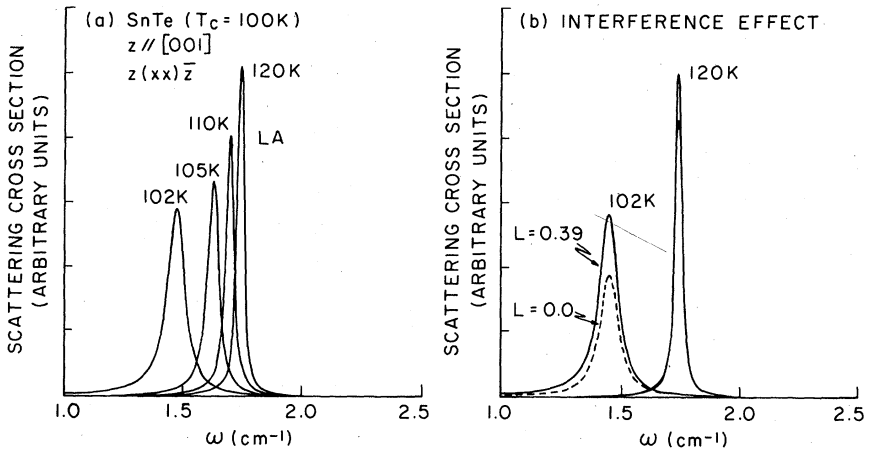

FIG. 6. (a) Temperature dependence of the calculated line-shape function $I_{LA}(Q,\Omega)$ according to Eq. (4.1) from the cubic (001) surface. (b) Interference effect between the Brillouin process and second-order Raman process at $T=102$ and 120 K. The interference parameter is chosen as $L=0.39$ cm^2.

width. This is a consequence of coupling to the two-phonon manifold, which broadens and softens as T_c is approached. In Fig. 6(b) the full and broken lines show the curves in the presence ($L=0.39$ cm^2) and in the absence ($L=0$) of the interference effect at 102 and 120 K. The main influence of the interference effect here is simply to increase the integrated intensity of the LA feature in the spectrum. Below the bare LA phonon frequency $\omega_{LA}=1.8$ cm^{-1}, the interference is constructive, and weakly frequency dependent. In Figs. 7(a) and 7(b) we show the spectrum from the (111) surface calculated from Eq. (4.5). In order to depict together the spectrum due to the LA mode and TA mode we magnify the intensity of the TA spectrum by a factor of 10. Note that the intensity of the spectrum *increases* as the temperature *decreases*. The tendency is opposite to that of the LA phonon spectrum from the (001) surface, as illustrated in Fig. 6(a). In Fig. 7 the Fano interference interference factors are assumed to be $L'_{LA}=0.39$ cm^2 and $L'_{TA}=-40$ cm^2. As is seen in Fig. 7(b) where the effects of interference are explicitly explored, the effect increases the intensity of the spectrum due to the TA mode dramatically and works constructively for the spectrum due to LA mode.

2. *Behavior below T_c*

The spectra from the (001) surface for the backward scattering geometry below T_c come from the LA and TA modes propagating along the c axis. The soft TO phonon with the polarization vector $\hat{e}_y(Q)$ or $\hat{e}_x(Q)$ also contributes to the spectrum. The expression for the line-shape function due to these modes is given by

$$S_j(Q,\Omega)=2\hbar[1+n(\Omega)]\frac{Q^2}{4\rho}K_j'^2[1+L_{1j}(\omega_{1j}^2-\Omega^2)+L_{2j}(\omega_{2j}^2-\Omega^2)]^2$$
$$\times(\epsilon_j)^2\left[-\mathrm{Im}\left(\Omega^2-\omega_j^2+\frac{Q^2}{9\rho}\Phi_j^2\langle Q_0\rangle^2\frac{1}{\omega_{TO}^2-\Omega^2-2i\Omega\Gamma}+\frac{Q^2}{4\rho}g_j'^2\Pi_0(Q,\Omega)\right)^{-1}\right]. \quad (4.9)$$

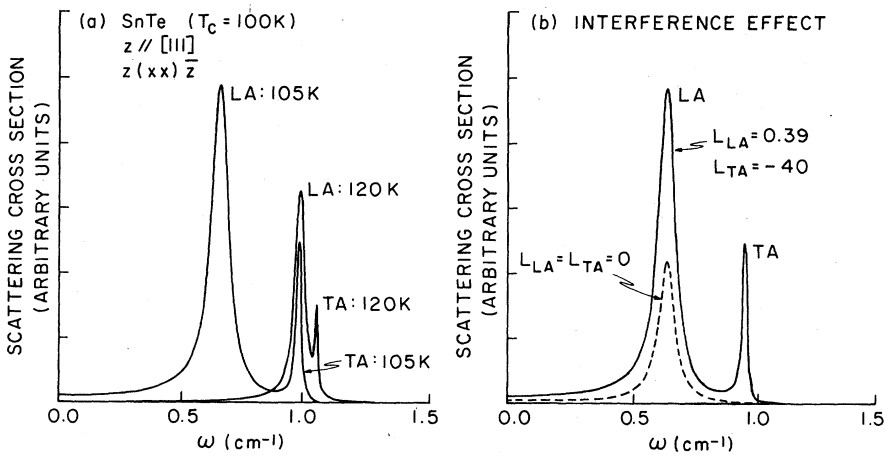

FIG. 7. (a) Temperature dependence of the calculated scattering spectrum due to the LA and TA modes from the (111) surface. (b) Interference effect in the line shape at $T=105$ K. The solid and broken lines represent in the presence ($L'_{LA}=0.39$ cm^2, $L'_{TA}=-40$ cm^2) and in the absence of this effect.

When the index j refers to the LA mode, we obtain

$$K_{\mathrm{LA}}^{r} = K_{12}^{r}\,, \tag{4.10a}$$

$$\epsilon_{\mathrm{LA}} = \hat{\epsilon}_{zz}\,, \tag{4.10b}$$

$$L_{1\mathrm{LA}} = 0\,, \tag{4.10c}$$

$$L_{2\mathrm{LA}} = -\frac{[(A_{11}+A_{12})\Phi_{31}+A_{13}\Phi_{33}]\rho V}{9g_{\mathrm{LA}}'^{2}Q^{2}K_{\mathrm{LA}}^{r}}\,, \tag{4.10d}$$

$$\Phi_{\mathrm{LA}} = 0\,, \tag{4.10e}$$

$$g_{\mathrm{LA}}'^{2} = \tfrac{1}{9}(2\Phi_{31}^{2}+\Phi_{33}^{2})\,, \tag{4.10f}$$

and frequencies

$$\omega_{1\mathrm{LA}}^{2} = \omega_{\mathrm{LA}}^{2} - (Q^{2}/4\rho)g_{\mathrm{LA}}'^{2}\mathrm{Re}\Pi_{0}(Q,\Omega)\,, \tag{4.10g}$$

$$\omega_{2\mathrm{LA}}^{2} = \omega_{\mathrm{LA}}^{2}\,. \tag{4.10h}$$

For the TA mode, we find

$$K_{\mathrm{TA}}^{r} = K_{14}^{r}\,, \tag{4.11a}$$

$$\epsilon_{\mathrm{TA}} = 2\hat{\epsilon}_{yz}\,, \tag{4.11b}$$

$$L_{1\mathrm{TA}} = -A_{14}\rho V/K_{\mathrm{TA}}^{r}Q^{2}\Phi_{44}\,, \tag{4.11c}$$

$$L_{2\mathrm{TA}} = -\frac{[(A_{11}-A_{12})\Phi_{41}+2A_{12}\Phi_{44}]\rho V}{9K_{14}^{r}g_{\mathrm{TA}}'^{2}Q^{2}}\,, \tag{4.11d}$$

$$g_{\mathrm{TA}}'^{2} = \tfrac{2}{9}(\Phi_{44}^{2}+\Phi_{41}^{2})\,, \tag{4.11e}$$

$$\Phi_{\mathrm{TA}} = \Phi_{44}\,. \tag{4.11f}$$

and frequencies

$$\omega_{1\mathrm{TA}}^{2} = \omega_{\mathrm{TA}}^{2} - (Q^{2}/4\rho)g_{\mathrm{TA}}'^{2}\mathrm{Re}\Pi_{0}(Q,\Omega)\,, \tag{4.11g}$$

$$\omega_{2\mathrm{TA}}^{2} = \omega_{\mathrm{TA}}^{2} + \frac{Q^{2}}{9\rho}\langle Q_{0}\rangle^{2}\Phi_{44}^{2}\frac{\Omega^{2}-\omega_{\mathrm{TO}}^{2}(Q)}{(\Omega^{2}-\omega_{\mathrm{TO}}^{2})^{2}+4\Omega^{2}\Gamma^{2}}\,, \tag{4.11h}$$

The contribution due to the TA mode for the $z(xy)\bar{z}$ configuration will be obtained by replacing the polarization vector $2\hat{\epsilon}_{yz}$ in (4.11b) by $2\hat{\epsilon}_{xz}$.

In Fig. 8 we plot the functions $I_{\mathrm{LA}}(Q,\Omega) + 10I_{\mathrm{TA}}(Q,\Omega)$ and $I_{\mathrm{TA}}(Q,\Omega)$ for the two scattering geometries. Again, the factor of 10 is included to artificially enhance the rather weak scattering from the TA mode. Our assumed values for the ratio $p_{11}:p_{12}:p_{44}$ produce a rather small value for $(p_{11}-p_{12}-2p_{14})$, which controls the intensity of the TA scattering. The values of the electrostrictive constant are supposed to be the same values as one above T_c. The temperature variation of the order parameter (sublattice displacement) is taken into account by employing Eq. (2.14).

As mentioned earlier, first-order Raman scattering from the TO phonon is allowed in the low-temperature phase. This mode appears in Fig. 8(a) as a broad feature near 15 cm^{-1}, and in Fig. 8(b) we see the TO frequency sink to zero as TO is approached from below. The Brillouin lines from the TA and LA modes have a strong Fano interference structure. In Fig. 8(b) we show the temperature variation of the interference structure near the TA mode frequency for the $z(xy)\bar{z}$ configuration where the spectrum due to the LA mode is forbidden. The TA mode is now broadened, and interferes with the two-phonon background combined with piezoelectric coupling to the optical motion. This coupling produces strong asymmetry of line which becomes steep as the temperature approaches T_c.

B. Effect of the opacity and integrated intensity

The frequency of Ar-ion laser line is above the fundamental absorption edge of SnTe, and consequently the real and imaginary parts n and K of the index of refraction are of comparable magnitude,[15] as listed in Table II. This gives rise to a very small skin depth (~100 Å), so that the observation of Raman-Brillouin spectrum from this material becomes difficult due to the reduction of the scattering efficiency. Theoretically, we can take into account this effect through simple con-

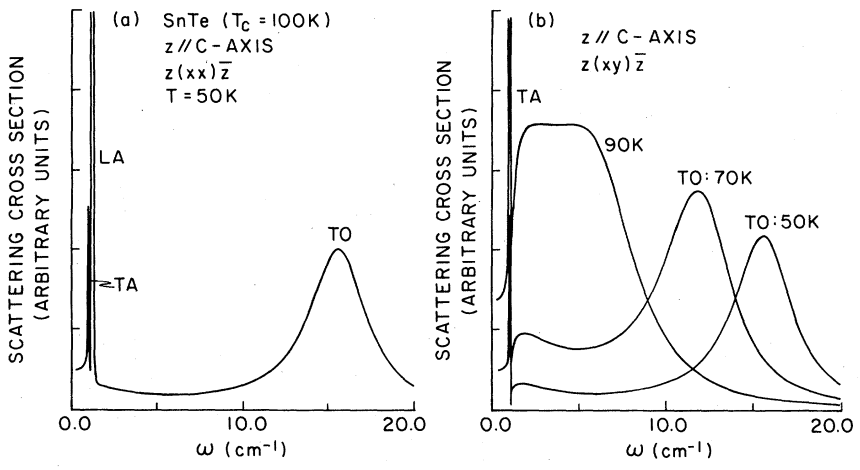

FIG. 8. (a) Calculated scattering spectrum at T = 50 K for the $z(xx)\bar{z}$ scattering geometry. There appears a strong Fano interference effect. (b) The temperature variation of the calculated scattering spectrum at the $z(xy)\bar{z}$ scattering geometry.

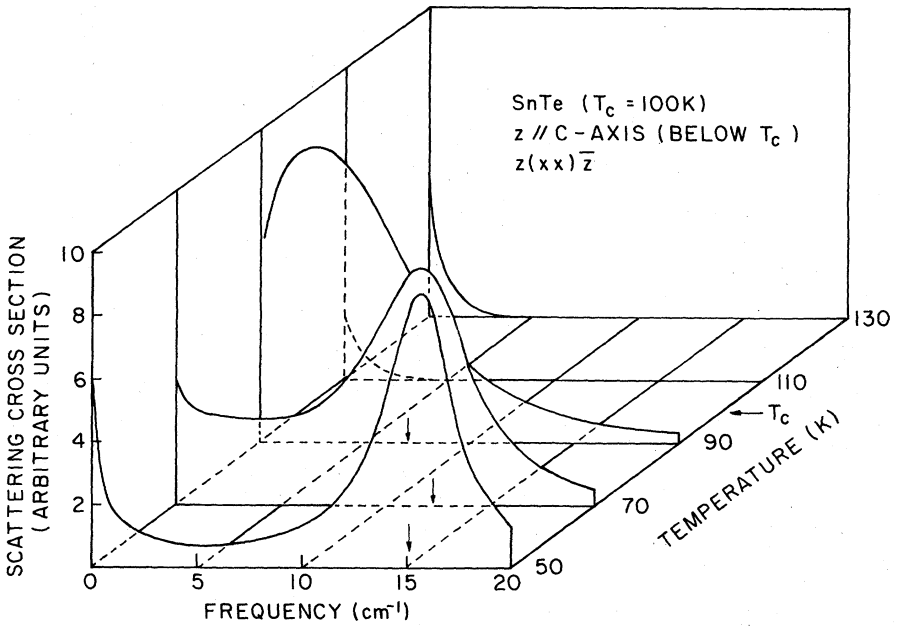

FIG. 9. Raman-Brillouin spectrum from the rhombohedral (001) surface calculated according to Eq. (4.12) under opaque conditions for both temperatures below and above T_c. The arrow is directed at the frequency of the soft TO phonon.

volution procedure over the momentum distribution. From Eq. (3.20) we calculate

$$\mathcal{S}_j(\Omega) = \int_0^\infty \frac{dQ}{2\pi} \frac{1}{(Q - \langle Q \rangle)^2 + (\Delta Q)^2} \mathcal{S}_j(Q, \Omega) , \tag{4.12}$$

with

$$\langle Q \rangle = (4\pi/\lambda) n , \tag{4.13a}$$

$$\Delta Q = (4\pi/\lambda) K . \tag{4.13b}$$

In Fig. 9 we plot the function $\mathcal{S}_j(\Omega)$ for frequency with temperatures below and above T_c from rhombohedral (001) surface below T_c [i.e., (111) surface above T_c]. This predicts the scattering spectrum from opaque SnTe, one should observe under realistic experimental conditions.

There appears two significant features in the spectrum below T_c. One of them is the drastic modification of the spectrum near Brillouin regime. The interference structure in Fig. 8(a) is completely smeared out, and instead of it the sharp winglike structure appears. This spectrum originates from the steep dispersion of the acoustic modes. However, as the soft mode drops into the Brillouin regine, there appears a broad peak whose position does not correspond to the soft-mode frequency (see the curve for 90K). Another important feature is that there is not such a big change in the spectrum near the soft TO frequency, except the reduction of its overall intensity. This is due to the weakness of the dispersion of the TO mode compared with acoustical phonons.

Finally we show the temperature dependence of the calculated integrated scattering intensity of the Raman-Brillouin spectrum. From Eq. (3.1) by taking account of the refractive index[10,11] we have

$$\left.\frac{dS}{d\Omega}\right|_{\text{Raman-Brillouin}} \cong \left(\frac{\omega_s}{c}\right)^4 \frac{1}{(\epsilon_1^2 + \epsilon_2^2)^{1/2}} \times \frac{K_j^2}{\rho} \int d\Omega \, \mathcal{S}_j(\Omega) , \tag{4.14}$$

where ϵ_1 and ϵ_2 are the real and imaginary part of the dielectric constant, respectively. In Fig. 10, where for the five temperatures used in the earlier spectra, we plot the integrated intensity of the Raman-Brillouin spectrum from Eq. (4.14).

We find that the integrated Raman-Brillouin intensity diverges as the temperature approaches T_c from below, and abruptly decreases when one passes T_c. The absolute magnitude of the integrated intensity is of order of 10^{-10} for our model parameters, with absorption included in the calculation.

V. CONCLUDING REMARKS

We have presented the theory of light scattering from the soft modes in the near vicinity of the phase transition temperature in IV-VI compound semiconductors. In order to describe the temperature variation of the order parameters, we developed the thermodynamical mean field description for the displacive structural phase transition, with emphasis on the role of electrostrictive coupling. This coupling gives us the appearance of the static rhombohedral strain below T_c, and from fitting data on the magnitude of this strain, we

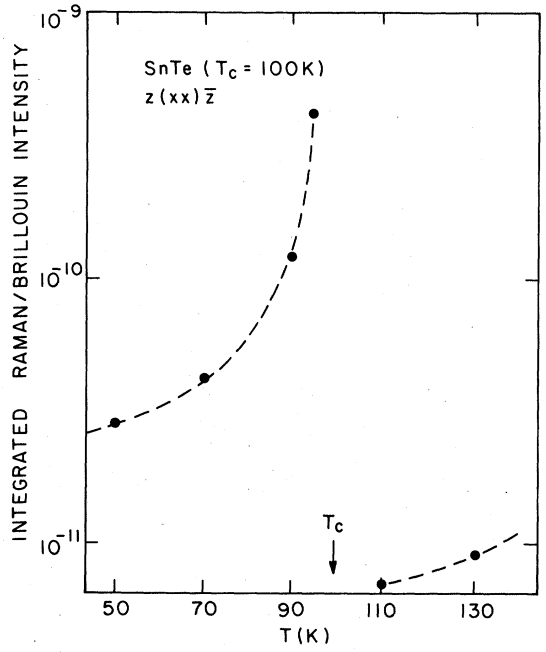

FIG. 10. Temperature variation of the integrated Raman-Brillouin intensity calculated according to Eq. (4.14).

determine the principal fundamental parameters of the model.

While there may be uncertainties associated with some of the parameters we have used in the calculation, we have been led to rather striking predictions; we see that below T_c, the prominent peak in the spectrum lies quite far from the frequency of the soft TO phonon, by virtue of the coupling to the acoustical mode and the two-phonon manifold. Also, we find a dramatic drop in integrated intensity as one moves above T_c. We hope our work will stimulate detailed studies of the structural phase transition of these materials by the light scattering method.

ACKNOWLEDGMENTS

The authors are grateful to Professor S. Ushioda for a number of discussions on the subject of this paper. One of us (S.K.) is indebted to Professor H. Kawamura, Professor K. Murase, and Dr. S. Sugai for initial discussions at Osaka University. He also wishes to thank Dr. R. Sirko for help with the numerical work. One of us (S.K.) would like to acknowledge support by the Nishina Foundation, and the other (D.L.M.) by U. S. Air Force Office of Scientific Research through Contract No. F49620-78-C-0019.

APPENDIX: EVALUATION OF THE PHONON PROPER SELF-ENERGY

The purpose of this Appendix is to derive the result quoted in Eq. (3.3). We begin by writing the second term of Eq. (3.10b) in the explicit form, denoting it by $\Pi_j^{(2)}(\vec{Q}, i\omega_m)$,

$$\Pi_j^{(2)}(\vec{Q}, i\omega_m) = \frac{2}{\beta}\sum_{ss'} |g_j(s,s')|^2 \sum_{\vec{q}, i\omega_{m'}} \frac{1}{\omega_{qs}^2 + \omega_{m'}^2 - \tilde{\Pi}_s(\vec{q}, i\omega_{m'})} \times \frac{1}{(\omega_{m'} - \omega_m)^2 + \omega_{\vec{Q}-\vec{q},s'}^2 - \tilde{\Pi}_{s'}(\vec{Q}-\vec{q}, i\omega_m - i\omega_{m'})} \tag{A1}$$

Here s and s' refer to soft TO modes, so in fact $\omega_{\vec{q}s}^2$ and the proper self energy are independent of s.

We begin by converting the sum on $i\omega_{m'}$ to an integral over real frequencies in the standard fashion. After doing this, we absorb the real part of the proper self-energy into a renormalized phonon frequency, presumed to be the experimentally measured mode frequency, and only the imaginary part is retained explicitly. If $n(\omega) = [\exp(\hbar\omega/k_BT) - 1]^{-1}$ is the Bose-Einstein function, the result can be written

$$\Pi_j^{(2)}(\vec{Q}, \Omega + i\epsilon) = 4\frac{2g_j^2\hbar}{\pi V}\sum_{\vec{q}} \int_{-\infty}^{+\infty} \frac{d\omega n(\omega)\omega\Gamma_q(\omega)}{(\omega_q^2 - \omega^2)^2 + 4\omega^2\Gamma_q^2(\omega)} \times \left(\frac{1}{\omega_{\vec{Q}-\vec{q}}^2 - (\Omega-\omega)^2 - 2i(\Omega-\omega)\Gamma_{\vec{Q}-\vec{q}}(\Omega-\omega)} + \frac{1}{\omega_{\vec{Q}+\vec{q}}^2 - (\Omega+\omega)^2 - 2i(\Omega+\omega)\Gamma_{\vec{Q}+\vec{q}}(\Omega+\omega)} \right). \tag{A2}$$

Here $g_j^2 = \sum_{ss'} |g_j(ss')|^2$ is the coupling constant of the acoustical mode of polarization j with the two-phonon manifold. We have neglected the dependence of $|g_j(s,s')|^2$ on the direction of $\vec{q}$ and $\vec{Q}-\vec{q}$. This greatly simplifies the analysis. Also $\omega\Gamma_{\vec{q}}(\omega)$ is the imaginary part of the proper self-energy of the soft TO phonon of wave vector $\vec{q}$. Ultimately, we shall ignore the dependence of $\Gamma_{\vec{q}}(\omega)$ on both ω and the wave vector $\vec{q}$. After this, if we suppose that $\omega_q^2 = \omega_0^2(T) + Aq^2$, a model description of the soft TO phonon used in this text and earlier work,[6] the integration over the direction of $\vec{q}$ may be performed in Eq. (A2). This gives a result that may be written, after replacing the Bose-Einstein function by its high-temperature form $k_BT/\hbar\omega$,

$$\Pi_j(Q,\Omega+i\epsilon)=\frac{g_j^2 k_B T}{\pi^3 AQ}\int_0^\infty dq\,q\int_{-\infty}^{+\infty}\frac{d\omega\,\Gamma}{(\omega_q^2-\omega^2)^2+4\omega^2\Gamma^2}$$
$$\times\left(\ln\left|\frac{(\Omega-\omega)^2+2i(\Omega-\omega)\Gamma-\omega_{q-Q}^2}{(\Omega-\omega)^2+2i(\Omega-\omega)\Gamma-\omega_{q+Q}^2}\right|+\ln\left|\frac{(\Omega+\omega)^2+2i(\Omega+\omega)\Gamma-\omega_{q-Q}^2}{(\Omega+\omega)^2+2i(\Omega+\omega)\Gamma-\omega_{q+Q}^2}\right|\right). \tag{A3}$$

Now we let $Q\to 0$, and note the integrand on the right-hand side of Eq. (A3) is an even function of Ω. This gives, with $v_q=\partial\omega_q/\partial q$,

$$\Pi_j(0,\Omega+i\epsilon)=\frac{4g_j^2 k_B T}{\pi^3 A}\int_0^\infty dq\;qv_q\omega_q\int_{-\infty}^{\infty}\frac{d\omega\,\Gamma}{(\omega_q^2-\omega^2)^2+4\omega^2\Gamma^2}$$
$$\times\left(\frac{1}{(\Omega-\omega)^2-\omega_q^2+2i(\Omega-\omega)\Gamma}+\frac{1}{(\Omega+\omega)^2-\omega_q^2+2i(\Omega+\omega)\Gamma}\right). \tag{A4}$$

The expression in large parentheses in Eq. (A4) is an even function of Ω. We then approximate the first factor in the integrand by

$$\Gamma/[(\omega_q^2-\omega^2)^2+4\omega^2\Gamma^2]\cong(1/4\omega_q^2)\{\Gamma/[(\omega_q-\omega)^2+\Gamma^2]+\Gamma/[(\omega_q+\omega)^2+\Gamma^2]\}, \tag{A5}$$

and approximation valid as long as $\Gamma<\omega_q$ (but Γ will not be small compared to Ω). The integration on ω may now be done in closed form to give

$$\Pi_j(0,\Omega+i\epsilon)=\frac{4g_j^2 k_B T}{\pi^2}\int_0^\infty\frac{dq\,q^2}{\omega_q^2}\,\frac{(\Omega+2i\Gamma)^2+\Gamma^2}{4\omega_q^2(\Omega+2i\Gamma)^2-[(\Omega+2i\Gamma)^2+\Gamma^2]^2}. \tag{A6}$$

In Eq. (A6), for $\Omega\ll\omega_q$ and Γ small compared to ω_q, the second term in the denominator is negligible. After some rearrangement, we get

$$\Pi_j(0,\Omega+i\epsilon)=\frac{g_j^2 k_B T}{\pi^2}\left(1+\frac{\Gamma^2}{(\Omega+2i\Gamma)^2}\right)\times\int_0^\infty\frac{dq\,q^2}{\omega_q^4}. \tag{A7}$$

The integral over q converges, with $\omega_q^2=\omega_0^2(T)+Aq^2$, demonstrating that the soft TO phonons contribute a separate, identifiable contribution to the proper self-energy, in the limit considered. The integral on q can be readily performed to give

$$\Pi_j(0,\Omega+i\epsilon)=\frac{g_j^2 k_B T}{4\pi A^{3/2}}\frac{1}{\omega_0(T)}\times\left(1+\frac{\Gamma^2}{(\Omega+2i\Gamma)^2}\right), \tag{A8}$$

a result equivalent to that displayed in Eq. (4.3).

Note that $T\to T_c$ and $\omega_0(T)$ vanishes, both the real and imaginary parts of Π_j diverge. This produces a strongly temperature-dependent renormalization of the sound velocity near T_c, after noting that g_j^2 is proportional to Q^2. Also, the attenuation varies strongly with T.

*Permanent address: Dept. of Physics, Osaka Univ., Toyonaka, Japan.

[1]P. A. Fleury, *Physical Acoustics*, edited by W. P. Mason (Academic, New York, 1970), Vol. VI, p. 1; J. F. Scott, Rev. Mod. Phys. 46, 83 (1974); and the references contained therein.

[2]The lattice distortions have the appropriate symmetry for the system to exhibit a macroscopic electric-dipole moment. However, the presence of free carriers screens out the moment, to render its direct observation impossible.

[3]H. Kawamura, Proceedings of the Third International Conference on the Physics of Narrow Band Gap Semiconductors, 1977 (unpublished); S. Katayama and H. Kawamura, Solid State Commun. 21, 521 (1977).

[4]L. J. Brillson, E. Burstein, and L. Muldawer, Phys. Rev. B 9, 1547 (1974); E. F. Steigmier and G. Harbeke, Solid State Commun. 8, 1275 (1970); S. Sugai, K. Murase, and H. Kawamura, *ibid.* 23, 127 (1977); T. Shimada, K. L. L. Kobayashi, Y. Katayama, and K. F. Komatsubara, Phys. Rev. Lett. 39, 143 (1977); S. Sugai, K. Murase, S. Katayama, T. Takaoka, S. Nishi, and H. Kawamura, Solid State Commun. 24, 407 (1977).

[5](a) W. Rehwald and G. K. Lang, J. Phys. C 8, 3287 (1975); (b) T. Seddon, S. C. Gupta, and G. A. Saunders, Phys. Lett. 56A, 45 (1976).

[6]R. E. Nettleton, Z. Phys. 220, 401 (1969); E. Pytte and J. Feder, Phys. Rev. 187, 1077 (1969).

[7]The displacement parameter δ is defined as $\delta=0.25-u$, where u is half the minimum distance between adjacent atoms along the [111] direction in units of the rhombohedral diagonal; $u=0.25$ for cubic phase and δ vanishes there.

[8]M. Iizumi, Y. Hamaguchi, K. F. Komatsubara, and Y. Kato, J. Phys. Soc. Jpn. 38, 443 (1975).

[9]L. Muldawer, J. Nonmetals 1, 177 (1973).

[10]D. L. Mills, A. A. Maradudin, and E. Burstein, Phys.

Rev. Lett. 21, 1178 (1968).
[11]M. Inoue and T. Moriya, J. Phys. Soc. Jpn. 29, 117 (1970).
[12]D. L. Mills and E. Burstein, Phys. Rev. 188, 1465 (1969).
[13]J. Shanker and S. K. Agarwal, J. Phys. Chem. Solids 37, 443 (1976).
[14]We model the ratios of the elements p_{ij} after KI, because in KI the ratios are close to those in the semiconductor GaAs. We are thus conjecturing the ratios to hold, at least approximately, for SnTe.
[15]M. Cardona and D. L. Greenaway, Phys. Rev. 133, 1685 (1964).